Roadmap of ellipsometric characterization of plasmonic nanoparticles

Yann Battie, Aotmane En Naciri

▶ **To cite this version:**

Yann Battie, Aotmane En Naciri. Roadmap of ellipsometric characterization of plasmonic nanoparticles. Journal of Vacuum Science & Technology B, Nanotechnology and Microelectronics, 2019, 37 (6), pp.062912. 10.1116/1.5121343 . hal-02899442

HAL Id: hal-02899442
https://hal.univ-lorraine.fr/hal-02899442

Submitted on 28 Jan 2022

HAL is a multi-disciplinary open access archive for the deposit and dissemination of scientific research documents, whether they are published or not. The documents may come from teaching and research institutions in France or abroad, or from public or private research centers.

L'archive ouverte pluridisciplinaire **HAL**, est destinée au dépôt et à la diffusion de documents scientifiques de niveau recherche, publiés ou non, émanant des établissements d'enseignement et de recherche français ou étrangers, des laboratoires publics ou privés.

ACCEPTED MANUSCRIPT
Journal of Vacuum Science Technology B
This is the author's peer reviewed, accepted manuscript. However, the online version of record will be different from this version once it has been copyedited and typeset.
PLEASE CITE THIS ARTICLE AS DOI: 10.1116/1.5121343

Roadmap of ellipsometric characterization of plasmonic nanoparticles

Yann Battie [1,a)] and Aotmane En Naciri [1]

[1] Laboratoire de Chimie et Physique - Approche Multi-échelles des milieux Complexes (LCP-A2MC), Université de Lorraine, 1 Boulevard Arago, 57078 Metz, France

[a)] Electronic mail: yann.battie@univ-lorraine.fr

This paper reports recent advances in ellipsometric characterization of silver and gold nanoparticles (NPs). Three systems are investigated: films composed of Au NPs distributed in shape, film with a gradient of concentration of Ag NPs and colloidal suspensions composed of Au NP chains. We show that ellipsometry is highly sensitive to the plasmon resonance of NPs. This latter can be used as an efficient probe of the NP morphology. The ellipsometric results are systematically compared to those obtained by transmission electron microscopy. We demonstrate that quantitative insights such as the shape distribution, the concentration and the organization of NPs can be extracted from ellipsometric spectra.

I. INTRODUCTION

Noble metallic nanoparticles (NPs) have fascinating plasmonic properties which can be used to elaborate several devices such as optical filters[1], sensors[2], or polarization

ACCEPTED MANUSCRIPT
Journal of Vacuum Science Technology B
This is the author's peer reviewed, accepted manuscript. However, the online version of record will be different from this version once it has been copyedited and typeset.
PLEASE CITE THIS ARTICLE AS DOI: 10.1116/1.5121343

state generators[3]. These properties depend on the NP size[4], shape[5-6] and organization[7]. Usually, the NPs morphology and organization are characterized by transmission electron microscopy (TEM). Despite TEM gives an accurate estimation of the NP morphology, this technique is time consuming and generally requires complex sample preparation. These limitations make crucial the development of complementary non-local and non-destructive characterization tools. UV-Visible absorption spectroscopy provides qualitative insights on the NP size and shape. However, this technique is not sensitive to the real part of the effective refractive index of nanocomposite which is a key parameter to design and optimize optical devices. In addition, it cannot be exploited to determine the gradient of NP concentration in thin film. Generally, this latter is evaluated by using large facilities such Rutherford backscattering spectroscopy (RBS). However, RBS gives information about in-depth gradient of metal concentration, but this is not necessarily the same as the NP concentration excepted if all the metal is agglomerated into NPs.

Spectroscopic ellipsometry (SE) is an indirect characterization tool based on the measurement of the change of the polarization state of light after the reflection on the sample. SE requires a modeling step to determine the real part and imaginary part of refractive index. SE was previously used to investigate the growth of metallic NPs on silicon[8-11], or in a dielectric matrix[12-17]. However, classical modeling approach fails to extract information on the NP morphology. Recent progress in modeling offers new opportunities to evaluate the influence of the NP size or shape distribution on their optical properties[6,18-19]. Mueller matrix ellipsometry was used to investigate the shape of NPs organized into array[20-22]. As shown by Voloshenko *et al.*[20], the Mueller matrix symmetry and depolarization factor of this nanostructure are directly related to the NP size and shape.

ACCEPTED MANUSCRIPT
Journal of Vacuum Science Technology B
This is the author's peer reviewed, accepted manuscript. However, the online version of record will be different from this version once it has been copyedited and typeset.
PLEASE CITE THIS ARTICLE AS DOI: 10.1116/1.5121343

Rigorous electromagnetic methods such as finite element method, discrete dipole approximation or rigorous coupled wave analysis are often used to extract relevant information concerning the NP morphology from ellipsometric spectra. Despite these methods give accurate results and have a large range of validity, they require large computing resource and are time consuming. On the contrary, effective medium theory, which approximate a nanocomposite material as a homogeneous medium, allows fast calculation. However, this homogenization procedure can introduce some errors. This approach can be considered since the scattering cross section of the metal nanoparticle is negligible. To respect this condition, the nanoparticle size must be smaller than a fraction (~1/10) of the wavelength. Toudert *et al.*[18] have proposed an extension of effective medium theory to describe the optical properties of a two dimensional layer composed of ellipsoidal NPs distributed in shape. This model requires preliminary estimation of the pair correlation function of NPs by TEM. Pecharroman *et al.*[19] have used the Bergman formalism to evaluate the spectral representation function (SRF) of NPs from SE measurements. However, the interpretation of SRF remains complex since it depends on a large number of parameters such as the NP shape, size, and organization. We have also generalized the classical Maxwell Garnett effective medium theory by introducing the NP shape distribution[6]. This shape distributed effective medium theory (SDEMT) was successively used to analyze absorption and ellipsometric measurements[13-14, 23-24].

In this paper, we report recent advances in SE characterization which suggest that SE is a valuable tool to determine simultaneously the optical properties, the shape distribution and the organization of plasmonic NPs. This paper gives an overview of our recent published papers. Thus, all data and samples presented in this paper have been

ACCEPTED MANUSCRIPT
Journal of Vacuum Science Technology B
This is the author's peer reviewed, accepted manuscript. However, the online version of record will be different from this version once it has been copyedited and typeset.
PLEASE CITE THIS ARTICLE AS DOI: 10.1116/1.5121343

already published. The plasmon bands of NPs are used as efficient probes of NPs. This paper is separated in 3 sections. The first one is focused on the estimation of the morphology Au NPs. We show that the NP shape distribution can be evaluated from SE measurements by analyzing them with the SDEMT model. In the second section, we extend the SDEMT model to inhomogeneous nanocomposites which exhibit a gradient of NP concentration. We demonstrate that the depth profile concentration of Ag NPs can be deduced from SE. The third section concerns the characterization of nanostructures composed of Au NPs. The number of NPs in the structure can be deduced from ellipsometric spectra by analyzing them with a coupled dipole model (CDM).

II. EXPERIMENTAL

Three types of samples are investigated: Thin films composed of gold NPs embedded in a photoresist (FAu_1 and FAu_2), thin film of silica which contains silver NPs (FAg) and colloidal suspensions (SAu_1, SAu_2) which contained Au NPs chains in water.

FAu_1 and FAu_2 are made as following: $HAuCl_4.3H_2O$ in propyleglycol monomethyl ether acetate is added to commercial AZ9260 photoresist. The mass fractions of gold salt in the photoresist are 5% and 60% for FAu_1 and FAu_2, respectively. After a 1 min sonication at room temperature, the mixture was deposited over cleaned silicon wafer by spin coating at 5000 rpm for 60s. To evaporate the solvent and initiate the growth of NPs, the films are baked 8 min at 80°C and 2 min at 120°C. The nominal volume fractions of Au NPs in FAu_1 and FAu_2, estimated from the concentration of precursor are 0.6% and 12%, respectively.

ACCEPTED MANUSCRIPT
Journal of Vacuum Science Technology B
This is the author's peer reviewed, accepted manuscript. However, the online version of record will be different from this version once it has been copyedited and typeset.
PLEASE CITE THIS ARTICLE AS DOI: 10.1116/1.5121343

FAg film is elaborated by ion implantation technique. A 250 nm thick SiO_2 film on Si substrate is implanted with silver ions. The silver ions dose and energy are 2.10^{16} cm^{-2} and 180 keV, respectively. The sample is then annealed 30 min at 300°C.

SAu_1 and SAu_2 suspensions are synthesized in 2 steps. First, a suspension of spherical Au NPs is elaborated by adding 0.492 ml of auric acid (0.486 mol/L) and 6 ml of sodium tricitrate (0.145 mol/L) to 500 mL of hot water. The solution is stirred 30 min to generate Au NPs with a diameter of 14 nm. Second, this suspension is destabilized by adding 95 µL and 100 µL of HCl (0.1 mol/L) for SAu_1 and SAu_2, respectively, in presence of 1.5 g of polyacrylic acid. Both suspensions are sonicated and then stirred overnight. The pH of the suspensions is then increased to 7 by introducing NaOH (1 mol/L). Finally, we remove the excess of polyacrylic acid by centrifugation.

TEM measurements on FAu_1, FAu_2 and FAg were performed with a Phillips CM200 microscope operating at 200 kV. To prepare FAu_1, FAu_2 TEM grids, the films are stripped off the substrate by scratching the samples with a razor blade. The film fragments are then deposited on a copper TEM grid. The FAg TEM grid is elaborated by cross-section focused ion beam lift-out technique. TEM images on SAu_1 and SAu_2 are recorded with a Philips EM 120 electron microscope operating at 120 kV. Drops of suspension were evaporated on carbon films coated 200/400 mesh copper grids.

SE allows determining the ellipsometric angles Ψ and Δ. These angles depend on the ratio of the complex Fresnel coefficients, r_p and r_s :

$$\frac{r_p}{r_s} = tan\Psi e^{j\Delta} \quad (1).$$

ACCEPTED MANUSCRIPT
Journal of Vacuum Science Technology B
This is the author's peer reviewed, accepted manuscript. However, the online version of record will be different from this version once it has been copyedited and typeset.
PLEASE CITE THIS ARTICLE AS DOI: 10.1116/1.5121343

SE measurements were performed with a phase-modulated ellipsometer (UVISEL, HORIBA). This ellipsometer measures two parameters I_s and I_c which depend on the ellipsometric angles Ψ and Δ:

$$I_s = sin2\Psi\ sin\Delta, \quad (2)$$

$$I_c = sin2\Psi\ cos\Delta. \quad (3)$$

In the case of thin films, the measurements are recorded at 3 angles of incidence: 50°, 60° and 70°. Suspensions are characterized by using a specific ellipsometric cell at 55°. The principle of this ellipsometric cell is given in references[25-27].

III. RESULTS AND DISCUSSION

A. Determination of the NP shape distribution

TEM image (Figure 1) reveals that FAu_1 NPs have spherical shape with a diameter estimated to 4 nm. On the contrary, FAu_2 NPs exhibit a broader shape distribution. Indeed, their aspect ratio is in the 0.5-1 range. Most of them are elongated. Indeed, the amount of spherical NPs (i.e. NPs whose aspect ratio is in the 0.95-1 range) decreases from 86% for FAu_1 to 30% for FAu_2. The mean diameter of FAu_2 NPs is estimated to 12 nm.

ACCEPTED MANUSCRIPT
Journal of Vacuum Science Technology B
This is the author's peer reviewed, accepted manuscript. However, the online version of record will be different from this version once it has been copyedited and typeset.
PLEASE CITE THIS ARTICLE AS DOI: 10.1116/1.5121343

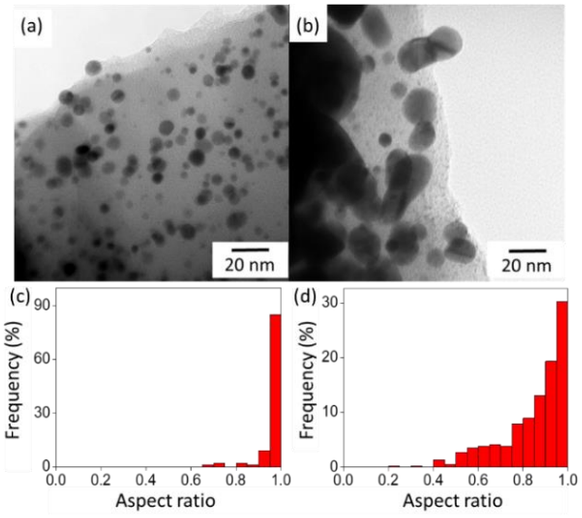

FIG. 1. (a)(b) TEM images and (c)(d) aspect ratio distributions of (a)(c) FAu_1, (b)(d) FAu_2. The aspect ratio distributions are estimated over 300 NPs.

We explore the ability of SE to characterize plasmonic NPs distributed in shape. Figure 2 shows the ellipsometric spectra of FAu_1 and FAu_2. To extract the optical properties of the film, the ellipsometric spectra are analyzed with a model which consists in a silicon substrate covered by a nanocomposite film. As reported in our previous papers[13-15], the films which are composed of randomly oriented ellipsoidal NPs embedded in a matrix, can be considered as homogeneous materials described by an effective dielectric function ε_{eff} given by the SDEMT model:

$$\varepsilon_{eff} = \frac{(1-f)\varepsilon_m + f\varepsilon_{np}\langle\beta\rangle}{(1-f)+f\langle\beta\rangle}, \quad (4)$$

where f is the volume fraction of NPs. ε_m and ε_{np} are the dielectric function of the matrix and NPs, respectively. In the following, the dielectric functions of NPs are always assimilated to the bulk values of metals given by Palik[28].

ACCEPTED MANUSCRIPT
Journal of Vacuum Science Technology B
This is the author's peer reviewed, accepted manuscript. However, the online version of record will be different from this version once it has been copyedited and typeset.
PLEASE CITE THIS ARTICLE AS DOI: 10.1116/1.5121343

The coefficient β is defined as:

$$\beta = \frac{\varepsilon_m}{3}\sum_{i=1}^{3}\frac{1}{\varepsilon_m + L_i(\varepsilon_{np}-\varepsilon_m)}, \quad (5)$$

where L_i (i=1,2,3) are the depolarization parameters of NP. The depolarization parameters only depend on the NP shape. They can be deduced from the aspect ratio of ellipsoidal NPs[13]:

$$L_i = \frac{r_2 r_3}{2}\int_0^{+\infty}\frac{dq}{(q+r_i^2)\sqrt{(q+1)(q+r_2^2)(q+r_3^2)}}, \quad (6)$$

where $r_i = \frac{a_i}{a_1}$, the aspect ratio of NPs. $a_1 \geq a_2 \geq a_3$ are the lengths of the principal axes of ellipsoidal NPs. Equation 6 implies that the depolarization parameters must respect the following sum rule:

$$\sum_{i=1}^{3} L_i = 1. \quad (7)$$

Due to the NP shape distribution, each NP has its own set of depolarization parameters. Thus, we take into account the NP shape distribution by introducing the distribution $P(L_1, L_2)$ of depolarization parameters:

$$\langle\beta\rangle = \iint P(L_1, L_2)\beta \; dL_1 dL_2. \quad (8)$$

In the following, we assume that the depolarization parameters follow a Gaussian distribution:

$$P(L_1, L_2) = A\, e^{-0.5\sum_{i=1}^{3}\left(\frac{L_i-\overline{L_i}}{\sigma_i}\right)^2}, \quad (9)$$

where $\overline{L_i}$ and σ_i are the mean value and the standard deviation of L_i, respectively and A is the normalization constant.

ACCEPTED MANUSCRIPT
Journal of Vacuum Science Technology B
This is the author's peer reviewed, accepted manuscript. However, the online version of record will be different from this version once it has been copyedited and typeset.
PLEASE CITE THIS ARTICLE AS DOI: 10.1116/1.5121343

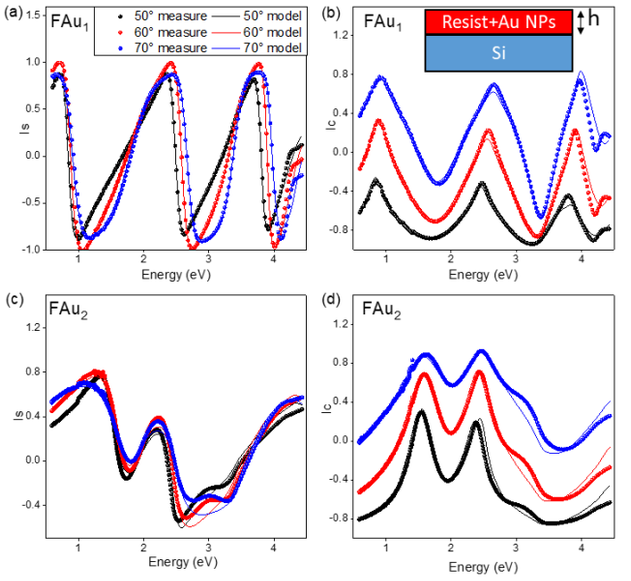

FIG. 2. (a)(b) Comparison between the measured (dots) and modeled ellipsometric (solid lines) spectra of FAu_1 and FAu_2. In inset of (b), the schematic description of the model used to analyze ellipsometric spectra

The SDEMT model is valid for NP size smaller than the wavelength. In addition, the volume fraction of NPs must be small enough to neglect the interaction between NPs. The refractive index of the matrix is set to the value of the photoresist. The film thickness, the volume fraction of NPs, the mean value and the standard deviation of depolarization factors of NPs are simultaneously fitted by using the Levenberg Marquardt algorithm[29]. As illustrated in Figure 2, the model reproduces the measured spectra. The fit results have a small sensitivity to the starting values of free parameters. Indeed, each free parameter has a specific impact on the spectra. This limits the correlation between free parameters. As we have shown in our previous work[6], the position and the number of plasmon bands depend on the mean value of depolarization factor while their width is directly related to σ_i. Their

ACCEPTED MANUSCRIPT
Journal of Vacuum Science Technology B
This is the author's peer reviewed, accepted manuscript. However, the online version of record will be different from this version once it has been copyedited and typeset.
PLEASE CITE THIS ARTICLE AS DOI: 10.1116/1.5121343

amplitude mainly depends on the volume fraction. The volume fraction of FAu_1 and FAu_2 NPs are estimated to 0.7% and 11%, respectively. These values are in accordance with the nominal ones calculated from the concentration of gold precursor, suggesting that the precursor is completely reduced during the heat treatment. In addition, the thicknesses of FAu_1 and FAu_2 estimated from SE are 258 nm and 105 nm, respectively. The thicknesses of FAu_1 and FAu_2 measured by mechanical profilometry are 249±14nm and 101±12nm, respectively. Thus, the thickness values estimated by SE are close to those obtained by mechanical profilometry, confirming the correctness of our model. The errors on $\overline{L_i}$, σ_i and f are smaller than $2x10^{-3}$, $3x10^{-3}$ and 10^{-3}, respectively. Thus, the high sensitivity of plasmon bands to the NPs shape ensures an accurate estimation of the NP shape distribution. The distributions of NP aspect ratio deduced from SE are shown in Figure 3(a)-(b). Contrary to classical TEM, which only gives a 2-dimensional projection of NPs, SE is sensitive to the two aspect ratio of NPs. The FAu_1 aspect ratio distribution found by SE is centered on the locus of spherical NPs (r_3=r_2=1). In accordance with TEM results, FAu_2 exhibits a broad NP shape distribution. Their aspect ratio is in the 0.5-1 range. Most of FAu_2 NPs are located on the locus of prolate NPs (r_3=r_2) confirming the presence of elongated NPs in the film. Unlike TEM measurements, SE is a nonlocal characterization tool which enables the determination of the NP shape distribution over a large number of NP. By considering the volume fraction of NPs and the film thickness, we estimate that the light beam probes approximately 10^{11} NPs. We conclude that SE combined with SDEMT can be used to determine the NP shape distribution.

Journal of Vacuum Science Technology B
ACCEPTED MANUSCRIPT
This is the author's peer reviewed, accepted manuscript. However, the online version of record will be different from this version once it has been copyedited and typeset.
PLEASE CITE THIS ARTICLE AS DOI: 10.1116/1.5121343

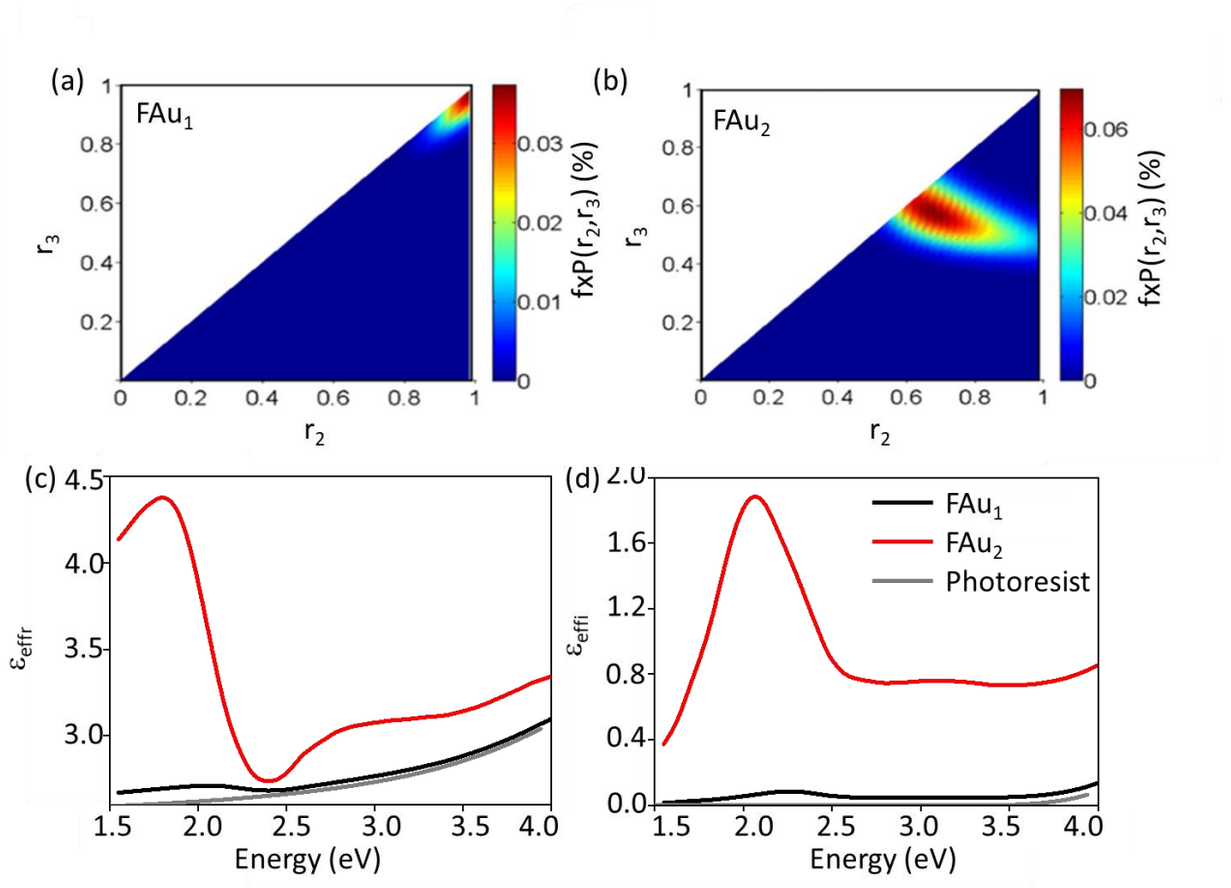

FIG. 3. Distribution of aspect ratio of (a) FAu_1 and (b) FAu_2 NPs determined by SE. (c) real part and (d) imaginary part of the effective dielectric function of FAu_1 and FAu_2 films. The dielectric function of the photoresist is also reported.

To evaluate the influence on the NP shape distribution on their optical properties, we report in Figure 3(c)-(d) the effective dielectric function of FAu_1 and FAu_2 films. Due to the contribution of the interband transitions of Au NPs, the imaginary part of dielectric function is almost constant in the 2.7 eV-4 eV spectral range. In addition, the imaginary part of the effective dielectric function of FAu_1 exhibits a plasmon band centered at 2.25 eV. In accordance to the Kramers Kronig relation[30], a large variation of the real part of the

ACCEPTED MANUSCRIPT
Journal of Vacuum Science Technology B
This is the author's peer reviewed, accepted manuscript. However, the online version of record will be different from this version once it has been copyedited and typeset.
PLEASE CITE THIS ARTICLE AS DOI: 10.1116/1.5121343

effective dielectric function is observed at the plasmon resonance. The plasmon band of FAu_1 is consistent with the plasmon frequency calculated based on the Fröhlich condition[31]. The plasmon band of FAu_2 is located at 2 eV. The increase of the NP size in FAu_2 is too small to explain this redshift. In addition, the volume fractions of NPs are sufficiently small to neglect the interaction between NPs. Thus, we attribute these spectral variations to the evolution of the NP shape distribution. The amplitude of the plasmon band of FAu_2 is 20 times higher than the plasmon band of FAu_1. Indeed, FAu_1 contains a smaller amount of Au NPs. We conclude that the NP shape distribution and the volume fraction of NPs have a strong impact on the optical properties of plasmonic nanocomposites, confirming that the plasmon band can be used as an efficient probe of the NP shape distribution. However, several conditions must be respected:

- The NP concentration must be small enough to neglect the NP interaction,
- the NP size must be sufficiently higher than few nm to neglect confinement effect[4],
- the NP size must be smaller than the wavelength to neglect scattering effect,
- the NPs must be embedded in a homogeneous dielectric matrix,
- the effect of interface on the plasmon band must be neglected.

B. Determination of the gradient of NP concentration in thin films

As shown in TEM image of FAg (Figure 4), ion implantation technique leads to the formation of spherical Ag NPs embedded in the SiO_2 matrix. Their diameter is in the 2 nm-20 nm range. A gradient of NP concentration is observed in the film depth. Most of NPs

ACCEPTED MANUSCRIPT
Journal of Vacuum Science Technology B
This is the author's peer reviewed, accepted manuscript. However, the online version of record will be different from this version once it has been copyedited and typeset.
PLEASE CITE THIS ARTICLE AS DOI: 10.1116/1.5121343

are located at a depth of 75 nm from the surface. In addition, a diffusion tail is also observed in the 90 nm-160 nm depth range.

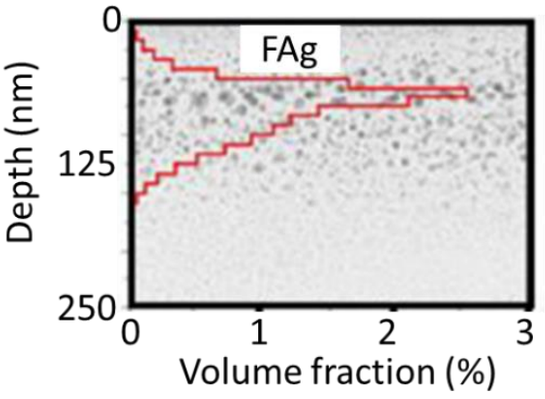

FIG. 4. TEM image of the cross section of FAg film. The red solid line is the gradient of volume fraction of Ag NPs found by SE.

Ellipsometric spectra, shown in Figure 5, exhibits several oscillations which come from the interference phenomena related to the multi-reflections in the silica layer. A physical model is established to extract the plasmonic responses of Ag NPs from the ellipsometric spectra. The model is composed of a silicon substrate covered by a silica film which contains Ag NPs. The thickness of the film is equal to 250 nm. To take into account the variation of the concentration of NPs in the film depth (t), the layer was divided into 30 sub-layers with equal thickness of 8.3 nm. Each sub-layer is thin enough, to consider the effective optical properties as constant. The effective dielectric function of each sub-layer is given by the SDEMT theory. We assume that the gradient of NP volume fraction is described by a bi-Gaussian distribution:

$$f(t) = \sum_{i=1}^{2} A_i e^{-0.5\left(\frac{t-t_{mi}}{\sigma_{ti}}\right)^2} . \quad (10)$$

ACCEPTED MANUSCRIPT
Journal of Vacuum Science Technology B
This is the author's peer reviewed, accepted manuscript. However, the online version of record will be different from this version once it has been copyedited and typeset.
PLEASE CITE THIS ARTICLE AS DOI: 10.1116/1.5121343

A_i, t_{mi} and σ_{ti} are the amplitude, the mean value and the standard deviation of each Gaussian term, respectively. The choice of this distribution is motivated by TEM and the fit quality of ellipsometric spectra. The free parameters $\overline{L_i}$ and σ_i, A_i, t_{mi} and σ_{ti} are fitted according the Levenberg-Marquardt algorithm. As shown in Figure 5, the model reproduces the measured ellipsometric spectra. In accordance with TEM, SE reveals that NPs have spherical shape. The gradient of NP volume fraction deduced from SE is reported on TEM image (Figure 4). This gradient is in agreement with TEM observation. Thus, SE can be used to evaluate the variation of NP concentration in the film. Compared to TEM, SE has several advantages. Indeed, ellipsometry is inexpensive and nondestructive technique which does not require sample preparation. Contrary to TEM, SE gives quantitative insight on the NP concentration. Finally, as illustrated in Figure 5, SE is sensitive to the gradient of dielectric function. As the deeper layers do not contain NP, their effective dielectric function is close to the dielectric function of SiO_2. On the contrary, in the 30 nm-150 nm depth range, the imaginary part of the effective dielectric function of the film is dominated by a plasmon band centered at 2.85 eV. According to the Fröhlich condition[31], this plasmon band is assigned to spherical Ag NPs. A large variation of the real part of the effective dielectric function occurs at the plasmon energy. The amplitude of the plasmon band is strongly correlated to the gradient of NP concentration. Indeed, the plasmon resonance is localized in the vicinity of the highly concentrated layer. These results argue that SE can be used to evaluate the variations of the plasmonic properties in the film depth.

ACCEPTED MANUSCRIPT
Journal of Vacuum Science Technology B
This is the author's peer reviewed, accepted manuscript. However, the online version of record will be different from this version once it has been copyedited and typeset.
PLEASE CITE THIS ARTICLE AS DOI: 10.1116/1.5121343

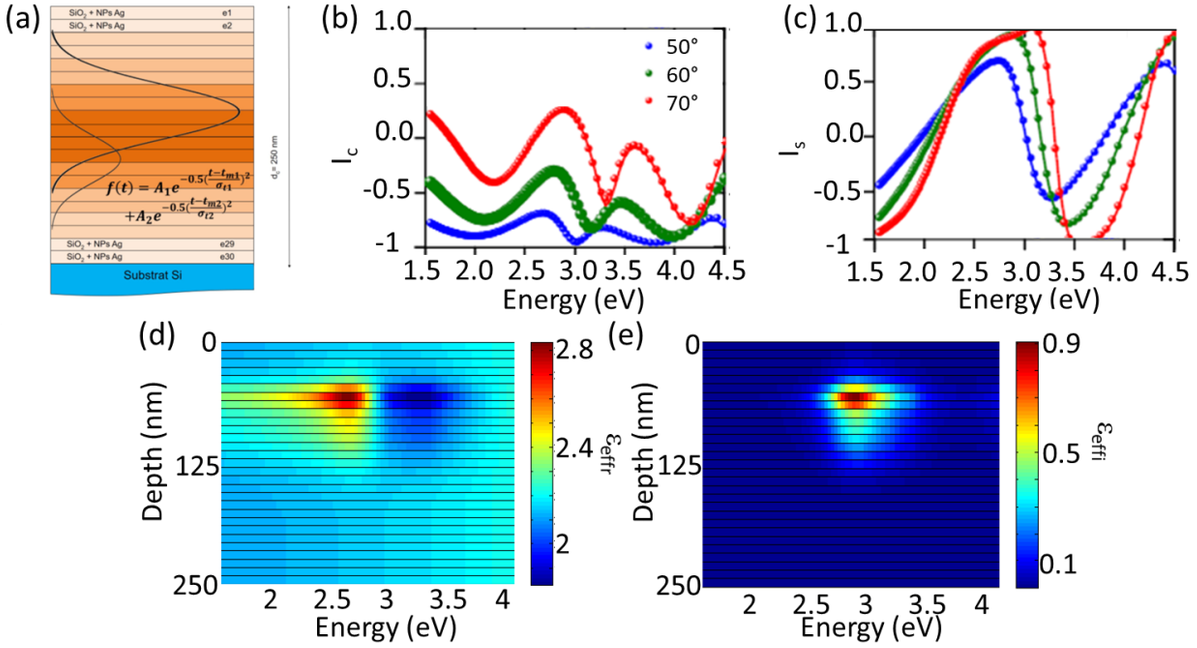

FIG. 5. (a) Schematic description of the model used to analyze ellipsometric spectra. (b)(c) Comparison between the measured (dots) and modeled (solid lines) ellipsometric spectra of FAg. (d)(e) variation of (d) the real part and (e) the imaginary part of the effective dielectric function with the film depth.

C. Determination of the number of NPs in plasmonic nanostructures

As shown by several authors[27, 32-33], NPs can be used as building blocks of plasmonic structures such as oligomers, chiral nanohelices or NP chains. Due to the strong interparticle coupling, the plasmon bands of these structures can be tuned in a broad spectral range by changing the organization and the distance between NPs[34-35]. In other words, the plasmon band contains relevant insight concerning the organization of NPs at

ACCEPTED MANUSCRIPT
Journal of Vacuum Science Technology B
This is the author's peer reviewed, accepted manuscript. However, the online version of record will be different from this version once it has been copyedited and typeset.
PLEASE CITE THIS ARTICLE AS DOI: 10.1116/1.5121343

nanoscale. In the following, two colloidal suspensions, denoted SAu_1 and SAu_2 are investigated. As shown in TEM images (Figure 6), the suspensions are composed of spherical gold NPs assembled into chains. The NP size is estimated to 7 nm while the interparticle distance is almost 1 nm. SAu_2 contains longer chain than SAu_1. Indeed, SAu_1 suspension mainly contains NP dimers while SAu_2 is composed of trimers and quadrimers.

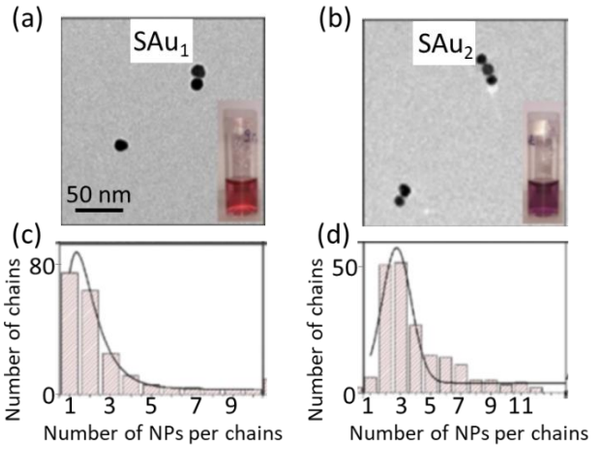

FIG. 6. (a)(b) TEM images of (a) SAu_1 and (b) SAu_2. The images of the suspensions are also given in inset. (c)(d) Distributions of the number of NPs per chains deduced from TEM in (c) SAu_1 and (d) SAu_2.

The measured SAu_1 and SAu_2 ellipsometric spectra are depicted in Figure 7 (a)-(b). The plasmonic behaviors of suspensions are clearly observed in the visible range of the Ic spectra. The complex refractive index of the suspensions is deduced from ellipsometric spectra by using a wavelength by wavelength inversion (Figure 7). Due to the low volume fraction of NPs, the real part of the refractive index is similar to the refractive index of water. Indeed, with our ellipsometric cell[25], the detection limit on imaginary part of refractive index is smaller than 10^{-6} while the detection limit on the real part of refractive index remain of the order of 10^{-3}. Thus, the presence of NPs in our suspension is only

ACCEPTED MANUSCRIPT
Journal of Vacuum Science Technology B
This is the author's peer reviewed, accepted manuscript. However, the online version of record will be different from this version once it has been copyedited and typeset.
PLEASE CITE THIS ARTICLE AS DOI: 10.1116/1.5121343

observe on the imaginary part of refractive index. The imaginary part of refractive index of SAu_1 is dominated by a broad and asymmetric plasmon band centered at 2.34 eV. On the other hand, the SAu_2 spectra has two plasmon bands located at 2.35 eV and 2.11 eV. These bands can be assigned to the longitudinal and the transversal plasmon modes of NP chains[36]. These modes can be selectively excited by an incident electric field parallel and perpendicular to the NP chains, respectively. As the NP size and shape are the same for both suspensions, the differences between the plasmonic properties of SAu_1 and SAu_2 can be attributed to the number of NPs in chain. This conclusion is supported by simulations performed on monodisperse NP chains, which reveal that an increase of the number of NP in chain induces a decrease of the energy of the longitudinal plasmon mode[27].

ACCEPTED MANUSCRIPT
Journal of Vacuum Science Technology B
This is the author's peer reviewed, accepted manuscript. However, the online version of record will be different from this version once it has been copyedited and typeset.
PLEASE CITE THIS ARTICLE AS DOI: 10.1116/1.5121343

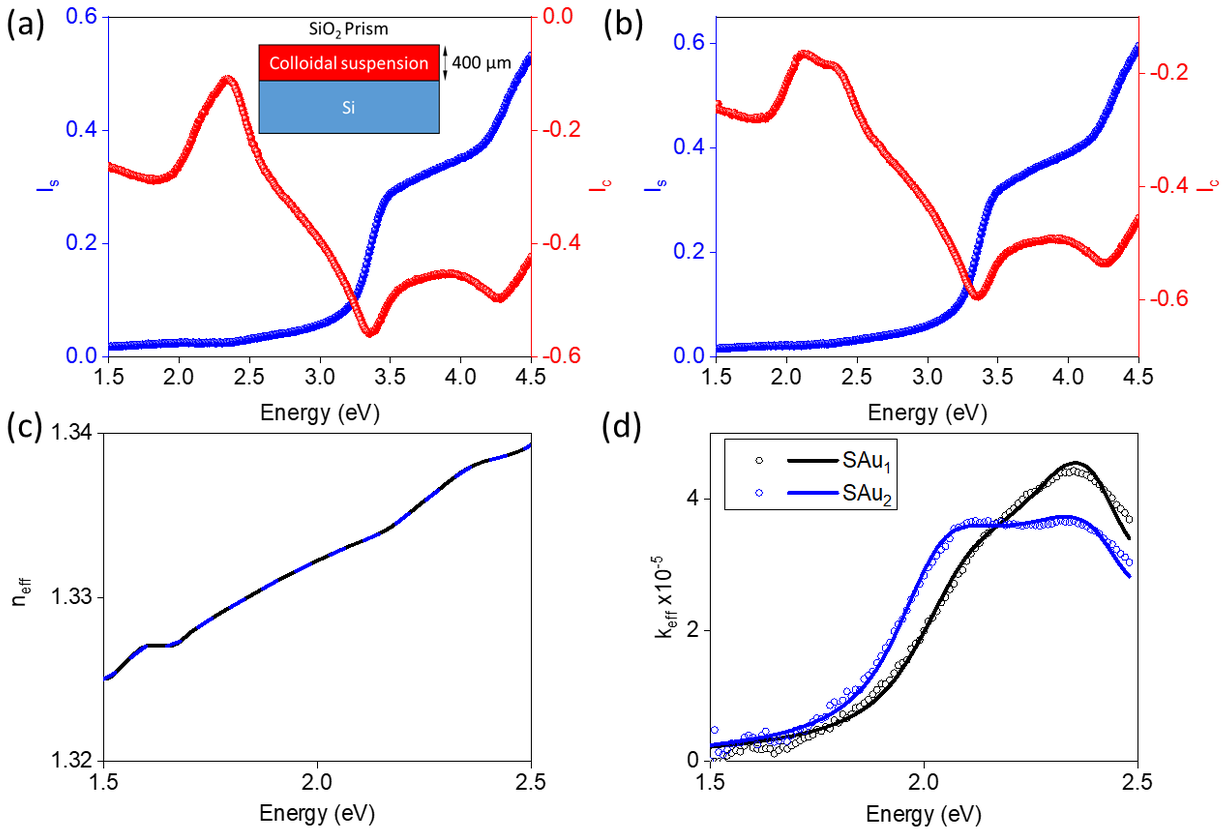

FIG. 7. (a)(b) Ellipsometric spectra of (a) SAu_1 and (b) SAu_2. In inset of (a), a schematic description of the model used to analyze the ellipsometric spectra. (c)(d) Effective index of SAu_1 and SAu_2 obtained by a wavelength by wavelength inversion (dots) and the coupled dipole method (solid lines).

To go further in the ellipsometric spectra analysis, we build a model, based on the coupled dipole method (CDM)[27], which takes into account the interaction between NPs. CDM considers each NP *m* located at a position $\overrightarrow{r_m}$, as a point dipole. As we have shown in our previous work[27], the optical properties of curved chains are similar to the optical

ACCEPTED MANUSCRIPT
Journal of Vacuum Science Technology B
This is the author's peer reviewed, accepted manuscript. However, the online version of record will be different from this version once it has been copyedited and typeset.
PLEASE CITE THIS ARTICLE AS DOI: 10.1116/1.5121343

properties of linear chains. By considering that NPs are in close contact limit, the NP positions are given by:

$$\overrightarrow{r_m} = 2R(m-1), \quad (11)$$

where R=7 nm is the mean value of NP radius measured by TEM. The NPs interact together through the scattered electromagnetic field. The dipole moment $\overrightarrow{P_m}$ of the NP m is given by:

$$\alpha^{-1}\overrightarrow{P_m} = \overrightarrow{E_0}e^{i\vec{k}\overrightarrow{r_m}} - \sum_{l\neq m}^{N_{np}} A_{ml}\overrightarrow{P_l}, \quad (12)$$

where α and N_{np} are the polarizability and the number of NPs in the structure, respectively. $\vec{k}$ and $\overrightarrow{E_0}$ are the wave vector and the amplitude vector of the incident electric field, respectively. The second term of Eq. (12) which describes the dipolar interaction between NPs, is given by:

$$A_{ml}\overrightarrow{P_l} = \frac{e^{ikr_{ml}}}{r_{ml}^3}\left\{k^2\overrightarrow{r_{ml}}\wedge\overrightarrow{r_{ml}}\wedge\overrightarrow{P_l} + \frac{1-jkr_{ml}}{r_{ml}^2}\left(r_{ml}^2\overrightarrow{P_l} - 3\overrightarrow{r_{ml}}\left(\overrightarrow{r_{ml}}.\overrightarrow{P_l}\right)\right)\right\}, \quad (13)$$

where $\overrightarrow{r_{ml}} = \overrightarrow{r_m} - \overrightarrow{r_l}$. By solving Eq. (12) for all NPs in the structures, we can calculate all dipole moments. The imaginary part of the effective refractive index of the suspension is expressed as:

$$\kappa = \frac{3}{2R^3|E_0|^2}\sum_{N_{np}=1}^{\infty}\frac{D(N_{np})}{N_{np}}\sum_{m=1}^{N_{np}}\overrightarrow{E_0}^{*}e^{-i\vec{k}\overrightarrow{r_m}}\overrightarrow{P_m}. \quad (14)$$

$D(N_{np})$ is the volume fraction distribution of chains composed of N_{np} NPs. In the following, we assume that $D(N_{np})$ is a bi-Gaussian distribution. To take into account random orientations of chains in suspension, κ is averaged over 30 orientations of the wave vector and polarization of the incident light according to the procedure described in our

ACCEPTED MANUSCRIPT
Journal of Vacuum Science Technology B
This is the author's peer reviewed, accepted manuscript. However, the online version of record will be different from this version once it has been copyedited and typeset.
PLEASE CITE THIS ARTICLE AS DOI: 10.1116/1.5121343

previous work[27]. The distribution $D(N_{np})$ is fitted according to the Levenberg-Marquart algorithm[29] by minimizing the root mean square error between the measured and the calculated imaginary part of effective refractive index of suspensions. As shown in Figure 7, the CDM reproduces the optical properties of the suspensions confirming that their plasmonic properties are strongly related to the interparticule interactions. The distributions of the number of NPs per chains estimated from ellipsometry, shown in Figure 8, are in accordance with those estimated by TEM. Indeed, SAu_2 contains longest chains than SAu_1. The small deviations with the distribution determined from TEM are attributed to the small number of chains probed by TEM. In addition, TEM is sensitive to the number of chains while ellipsometry is sensitive to volume occupied by each chain. The number of NP chains probed by ellipsometry, estimated to 10^{10}, is sufficiently significant to give an accurate estimation of the distribution of the number of NPs per chain. Finally, ellipsometry allows the determination of the volume fraction of chains. This latter is estimated to 13 ppmv and 18 ppmv for SAu_1 and SAu_2, respectively, suggesting that ellipsometry combined with a specific cell is sufficiently sensitive to detect small concentration of NPs[25-27].

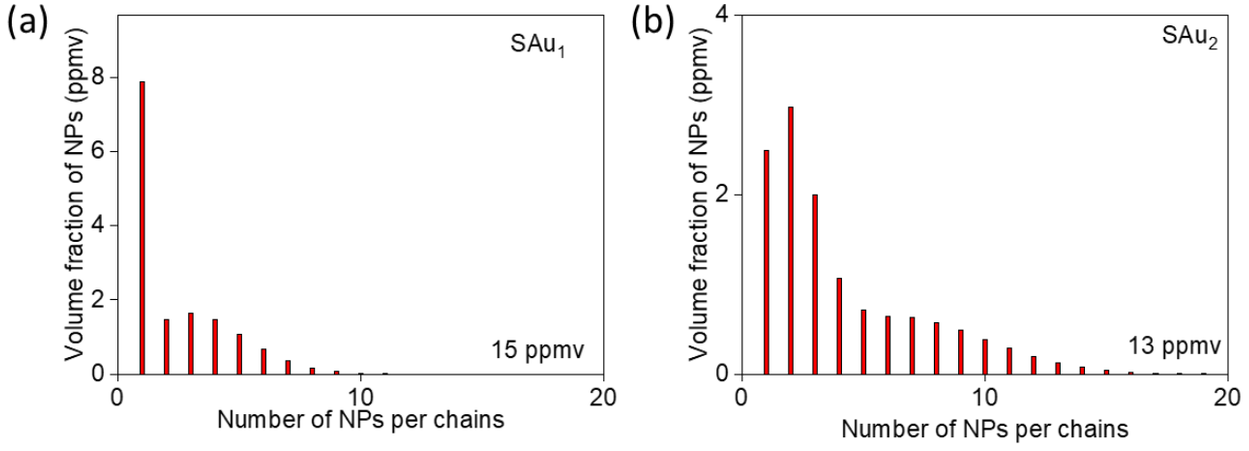

ACCEPTED MANUSCRIPT
Journal of Vacuum Science Technology B
This is the author's peer reviewed, accepted manuscript. However, the online version of record will be different from this version once it has been copyedited and typeset.
PLEASE CITE THIS ARTICLE AS DOI: 10.1116/1.5121343

FIG. 8. Distribution of the number of NPs per chains obtained by SE in (a) SAu_1 and (b) SAu_2.

IV. CONCLUSION

In summary, this paper argues the importance of SE for the metrology of plasmonic NPs. The shape distribution, the gradient of concentration of NPs as well as the number of NPs in nanostructures can be estimated by analyzing ellipsometric spectra with an adequate model such as SDEMT or CDM. This technique takes the advantage of the high sensitivity of SE and the strong dependence between plasmon band and the shape and organization of NPs. Since SE is a non-local characterization tool, this technique gives statistically significant distribution. Thus, SE can be considered as an alternative to TEM for the characterization of plasmonic materials. We now discuss the future trends of SE characterization of plasmonic NPs. With the improvement of the NP synthesis routes, more and more complex nanostructures are investigated such as alloy NPs[37], nanocubes[38], hollow NPs[39], or core-shell NPs[40]. We expect that all parameters which have a significant impact on the plasmonic resonance of NPs, such as the NP composition or shell thickness, can be determined from SE. In addition, nanostructure composed of self-assembled NPs can be used to manipulate the polarization of light. As the plasmon modes of anisotropic NPs can be selectively exited by specific polarization state of light, ellipsometry can be used to evaluate the orientation of NPs[41] or the chirality of nanostructure[42-43]. The challenge remains the development of models which capture the main physical properties of plasmonic nanostructures. Rigorous methods, based on the resolution of the Maxwell

ACCEPTED MANUSCRIPT
Journal of Vacuum Science Technology B
This is the author's peer reviewed, accepted manuscript. However, the online version of record will be different from this version once it has been copyedited and typeset.
PLEASE CITE THIS ARTICLE AS DOI: 10.1116/1.5121343

equation can be applied to a large number of nanostructures but require large computing resource. Other approaches based on homogenization procedures are less computing time consuming. However, their domain of validity is more restricted and new effective medium theory must be developed for each studied nanostructure.

ACKNOWLEDGMENTS

We would like to thank Dr Irene Izquierdo-Lorenzo, Dr Safi Jradi, and Dr Pierre Michel Adam from the Laboratory L2N (université technologique de Troyes) for the elaboration of FAu_1 and FAu_2 and their fruitful discussion. We would like to thank Dr Yann Le Gall, Dr Dominique Muller and Dr Daniel Mathiot from the Laboratory ICube (université de Strasbourg) for the elaboration of FAg and their fruitful discussion. We would like to thank Dr Jie Gao, Dr Emilie Pouget and Dr Reiko Oda of the CBMN laboratory (Université de Bordeaux) for the synthesis of SAu_1 and SAu_2 and their fruitful discussion. We thank the Ellipsometry core facility of LCP-A2MC (Université de Lorraine - http://lcp-a2mc.univ-lorraine.fr).

[1]L. Escoubas, M. Carlberg, J. Le Rouzo, F. Pourcin, J. Ackermann, O. Margeat, C. Reynaud, D. Duche, J.-J. Simon, R.-M. Sauvage, and G. Berginc, Prog. Quant. Electron0 **63**, 1-22 (2019).

[2]M. Li, S. K. Cushing, and N. Wu, Analyst **140**, 386-406 (2015).

[3]L. M. S. Aas, M. Kildemo, C. Martella, M. C. Giordano, D Chiappe, and F. Buatier de Mongeot, Opt. Express **21**, 30918-30931 (2013).

[4]Y. Battie, A. Resano-Garcia, N. Chaoui, Y. Zhang, and A. En Naciri, J. Chem. Phys. **140**, 044705 (2014).

[5]C. Noguez, J. Phys. Chem. C **111**, 3806-3819 (2007).

ACCEPTED MANUSCRIPT
Journal of Vacuum Science Technology B
This is the author's peer reviewed, accepted manuscript. However, the online version of record will be different from this version once it has been copyedited and typeset.
PLEASE CITE THIS ARTICLE AS DOI: 10.1116/1.5121343

[6]A. Resano-Garcia, Y. Battie, A. En Naciri, S. Akil, and N. Chaoui, J. Chem. Phys **142**, 134108 (2015).

[7]H. Cha, D. Lee, J. Hee Yoon, and S. Yoon, J. Colloid Interf. Sci. **464**, 18-24 (2016).

[8]Y. Battie, A. En Naciri, W. Chamorro, and D. Horwat, J. Phys. Chem. C **118**, 4899-4905 (2014).

[9]M. Losurdo, M. M. Giangregorio, G. V. Bianco, A. A. Suvorova, C. Kong, S. Rubanov, P. Capezzuto, J. Humlicek, and G. Bruno, Phys. Rev. B **82**, 155451 (2010).

[10]T. W. H. Oates, M. Ranjan, S. Facsko, and H. Arwin, Opt. Express **19**, 2014-2028, 2011.

[11]T.W.H. Oates, Appl. Surf. Sci. **258**, 9278-9282 (2012).

[12]Y. Battie, A. En Naciri, M. Vergnat, J. Appl. Phys. **122**, 213101 (2017).

[13]Y. Battie, I. Izquierdo-Lorenzo, A. Resano-Garcia, A. En Naciri, S. Akil, P. M. Adam, and S. Jradi, Appl. Surf. Sci. **421**, 301-309 (2017).

[14]Y. Battie, I. Izquierdo-Lorenzo, A. Resano-Garcia, A. En Naciri, S. Akil, P. M. Adam, and S. Jradi, J. Nanopart. Res. **18**, 217 (2016).

[15]Y. Battie, A. En Naciri, N. Chaoui, Y. Le Gall, D. Muller, M. Carrada, and D. Mathiot, J. Appl. Phys. **122**, 085308 (2017).

[16]T. W. H. Oates, Appl. Phys. Lett. **88**, 213115 (2006).

[17]T. W. H. Oates, and E. Christalle, J. Phys. Chem. C **111**, 182-187 (2007).

[18]J. Toudert, L. Simonot, S. Camelio, and D. Babonneau, Phys. Rev. B **86**, 045415 (2012).

[19]C. Pecharroman, E. Della Gaspera, A. Martucci, R. Escobar-Galindod, and P. Mulvaney, J. Phys. Chem. C **119**, 9450−9459 (2015).

[20]I. Voloshenko, B. Gompf, A. Berrier, M. Dressel, G. Schnoering, M. Rommel, and J. Weis, Appl. Phys. Lett. **115**, 063106 (2019).

[21]P. M. Walmsness, T. Brakstad, B. B. Svendsen, J.-P. Banon, J. C. Walmsley, and M. Kildemo, J. Opt. Soc. Am. B **36**, 78-87 (2019).

ACCEPTED MANUSCRIPT
Journal of Vacuum Science Technology B
This is the author's peer reviewed, accepted manuscript. However, the online version of record will be different from this version once it has been copyedited and typeset.
PLEASE CITE THIS ARTICLE AS DOI: 10.1116/1.5121343

[22]T. Brakstad, M. Kildemo, Z. Ghadyani, and I. Simonsen, Opt. Express **23**, 22800-22815 (2015).

[23]Y Battie, A Resano-Garcia, A En Naciri, S Akil, and N Chaoui, Appl. Phys. Lett. **107**, 143104 (2015).

[24]Y. Mansour, Y. Battie, A. En Naciri, and N. Chaoui, Opt. Lett. **44**, 3390-3393 (2019).

[25]M. Stchakovsky, Y. Battie, and A. En Naciri, Appl. Surf. Sci. **421**, 802-806 (2017).

[26]Y. Battie, M. Stchakovsky, A. En Naciri, S. Akil, N. Chaoui, and L. Broch, Langmuir **33**, 7425-7434 (2017).

[27]J. Vieaud, J. Gao, J. Cane, M. Stchakovsky, A. En Naciri, K. Ariga, R. Oda, E. Pouget, and Y. Battie, J. Phys. Chem. C **122**, 11973-11984 (2018).

[28]E.D. Palik, *Handbook of Optical Constants of Solids*, (Academic press handbook series, New York, 1985).

[29]K. Levenberg, Quart. Appl. Math. **2**, 164–168 (1944).

[30]R. L. Kronig, J. Opt. Soc. Am. **12**, 547–557 (1926).

[31]U. Kreibig, and M. Vollmer, *Optical properties of metal cluster* (Springer-Verlag Berlin, 1995).

[32]M. Esposito, F. Todisco, S. Bakhti, A. Passaseo, I. Tarantini, M. Cuscunà, N. Destouches, and V. Tasco, Nano Lett. **19**, 1922-1930 (2019).

[33]J. Cheng, G. Le Saux, J. Gao, T. Buffeteau, Y. Battie, P. Barois, V. Ponsinet, M.-H. Delville, O. Ersen, E. Pouget, and R. Oda, ACS Nano **11**, 3806-3818 (2017).

[34]I. Romero, J. Aizpurua, G. W. Bryant, and F. J. García de Abajo, Opt. Express **14**, 9988 (2006).

[35]L.L. Zhao, K. L. Kelly, and G. C. Schatz, J. Phys. Chem. B **107**, 7343-7350 (2003).

[36]P. K. Jain, and M. A. El-Sayed, Chem. Phys. Lett. **487**, 153-164 (2010).

ACCEPTED MANUSCRIPT
Journal of Vacuum Science Technology B
This is the author's peer reviewed, accepted manuscript. However, the online version of record will be different from this version once it has been copyedited and typeset.
PLEASE CITE THIS ARTICLE AS DOI: 10.1116/1.5121343

[37] O. Peña-Rodríguez, M. Caro, A. Rivera, J. Olivares, J. M. Perlado, and A. Caro, Opt. Mater. Express **4**, 403-410 (2014).

[38]R. Omar, A. En Naciri, S. Jradi, Y. Battie, J. Toufaily, H. Mortada, and S. Akil, J. Mater. Chem. C **5**, 10813-10821 (2017).

[39]D. Wan., H. L. Chen, Y.-S. Lin, S.-Y. Chuang, J. Shieh, and S.-H. Chen, ACS Nano **3**, 960-970 (2009).

[40]L. Malassis, P. Massé, M. Tréguer-Delapierre, S. Mornet, P. Weisbecker, P. Barois, C. R. Simovski, V. G. Kravets, and A. N. Grigorenko, Adv. Mater. **26**, 324–330 (2014).

[41]F. Borondics, E. Garcia-Caurel, Appl. Surf. Sci, **421**, 728-73 (2017).

[42]G. K. Larsen, and Y. Zhao, Appl. Phys. Lett. **105**, 071109 (2014).

[43]J. Cheng, G. Le Saux, J. Gao, T. Buffeteau, Y. Battie, P. Barois, V. Ponsinet, ACS Nano, **11**, 3806-3818 (2017).

ACCEPTED MANUSCRIPT
Journal of Vacuum Science Technology B
This is the author's peer reviewed, accepted manuscript. However, the online version of record will be different from this version once it has been copyedited and typeset.
PLEASE CITE THIS ARTICLE AS DOI: 10.1116/1.5121343

FIGURE CAPTIONS

FIG. 1. (a)(b) TEM images and (c)(d) aspect ratio distributions of (a)(c) FAu_1, (b)(d) FAu_2. The aspect ratio distributions are estimated over 300 NPs.

FIG. 2. (a)(b) Comparison between the measured (dots) and modeled ellipsometric (solid lines) spectra of FAu_1 and FAu_2. In inset of (b), the schematic description of the model used to analyze ellipsometric spectra

FIG. 3. Distribution of aspect ratio of (a) FAu_1 and (b) FAu_2 NPs determined by SE. (c) real part and (d) imaginary part of the effective dielectric function of FAu_1 and FAu_2 films. The dielectric function of the photoresist is also reported.

FIG. 4. TEM image of the cross section of FAg film. The red solid line is the gradient of volume fraction of Ag NPs found by SE.

FIG. 5. (a) Schematic description of the model used to analyze ellipsometric spectra. (b)(c) Comparison between the measured (dots) and modeled (solid lines) ellipsometric spectra of FAg. (d)(e) variation of (d) the real part and (e) the imaginary part of the effective dielectric function with the film depth.

FIG. 6. (a)(b) TEM images of (a) SAu_1 and (b) SAu_2. The images of the suspensions are also given in inset. (c)(d) Distributions of the number of NPs per chains deduced from TEM in (c) SAu_1 and (d) SAu_2.

FIG. 7. (a)(b) Ellipsometric spectra of (a) SAu_1 and (b) SAu_2. In inset of (a), a schematic description of the model used to analyze the ellipsometric spectra. (c)(d) Effective index

ACCEPTED MANUSCRIPT
Journal of Vacuum Science Technology B
This is the author's peer reviewed, accepted manuscript. However, the online version of record will be different from this version once it has been copyedited and typeset.
PLEASE CITE THIS ARTICLE AS DOI: 10.1116/1.5121343

of SAu_1 and SAu_2 obtained by a wavelength by wavelength inversion (dots) and the coupled dipole method (solid lines).

FIG. 8. Distribution of the number of NPs per chains obtained by SE in (a) SAu_1 and (b) SAu_2.

Journal of Vacuum Science Technology B

ACCEPTED MANUSCRIPT

This is the author's peer reviewed, accepted manuscript. However, the online version of record will be different from this version once it has been copyedited and typeset.
PLEASE CITE THIS ARTICLE AS DOI: 10.1116/1.5121343

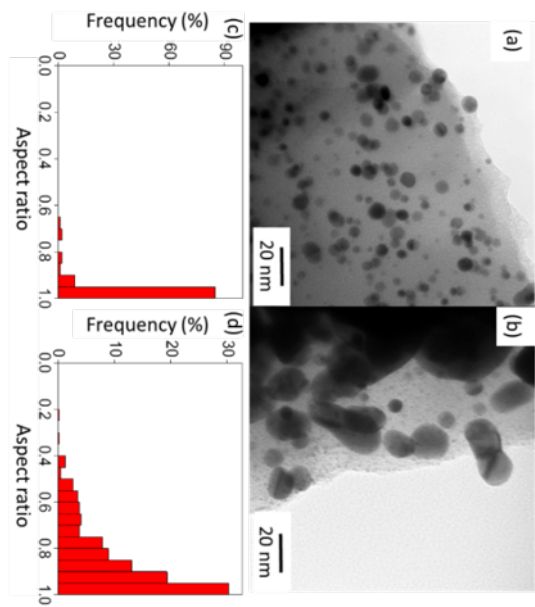

Journal of Vacuum Science Technology B

ACCEPTED MANUSCRIPT

This is the author's peer reviewed, accepted manuscript. However, the online version of record will be different from this version once it has been copyedited and typeset.
PLEASE CITE THIS ARTICLE AS DOI: 10.1116/1.5121343

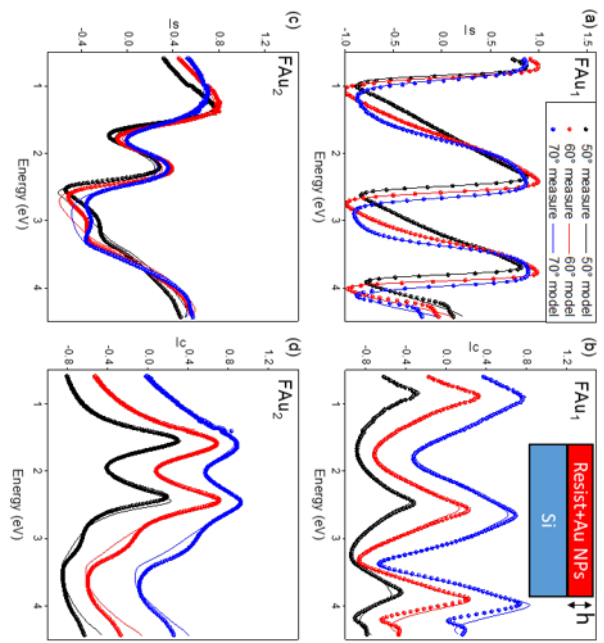

ACCEPTED MANUSCRIPT

Journal of Vacuum Science Technology B

This is the author's peer reviewed, accepted manuscript. However, the online version of record will be different from this version once it has been copyedited and typeset.
PLEASE CITE THIS ARTICLE AS DOI: 10.1116/1.5121343

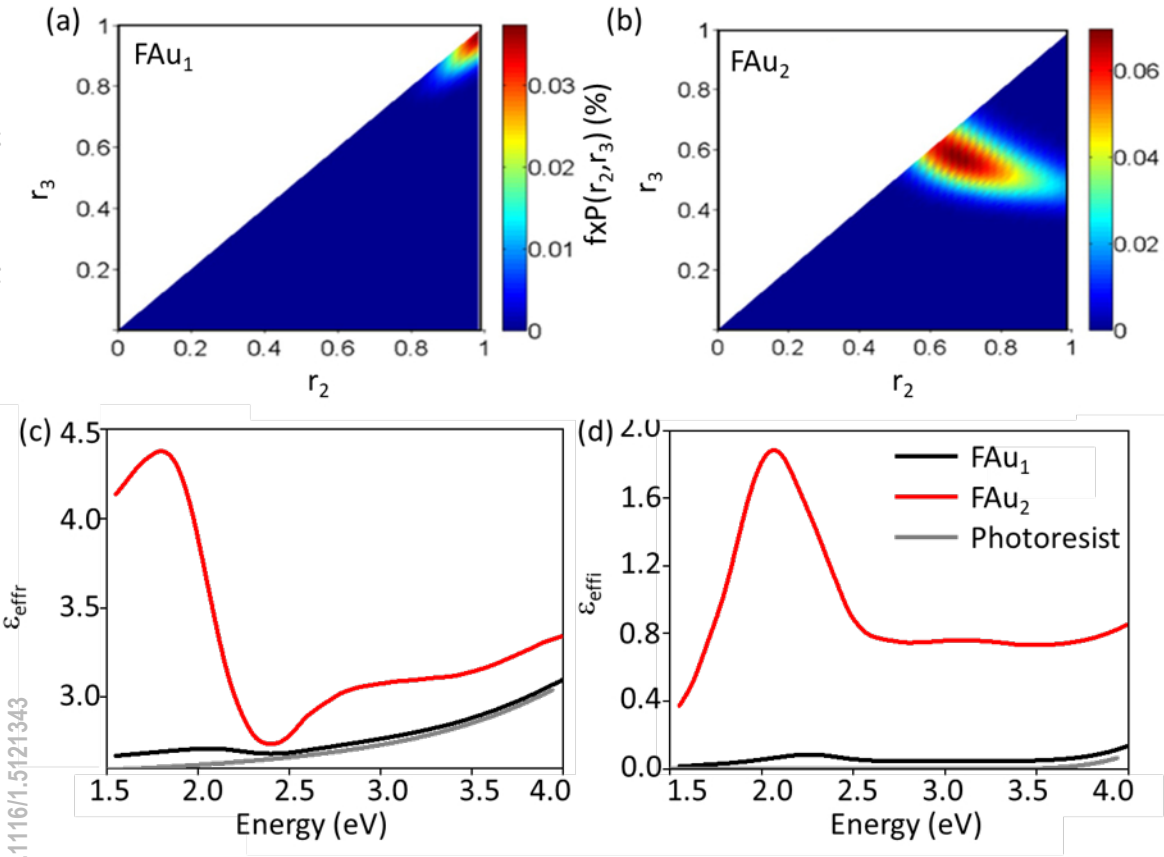

Journal of Vacuum Science Technology B

ACCEPTED MANUSCRIPT

This is the author's peer reviewed, accepted manuscript. However, the online version of record will be different from this version once it has been copyedited and typeset.
PLEASE CITE THIS ARTICLE AS DOI: 10.1116/1.5121343

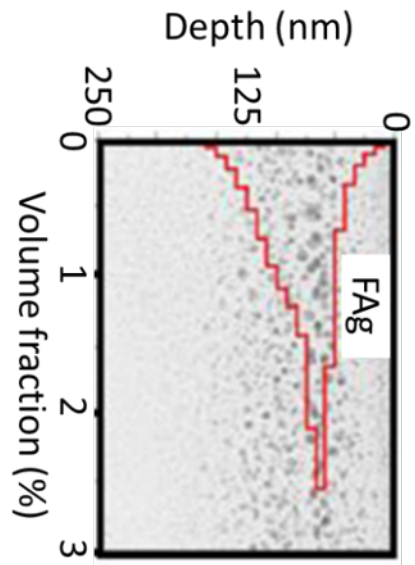

ACCEPTED MANUSCRIPT

Journal of Vacuum Science Technology B

This is the author's peer reviewed, accepted manuscript. However, the online version of record will be different from this version once it has been copyedited and typeset.
PLEASE CITE THIS ARTICLE AS DOI: 10.1116/1.5121343

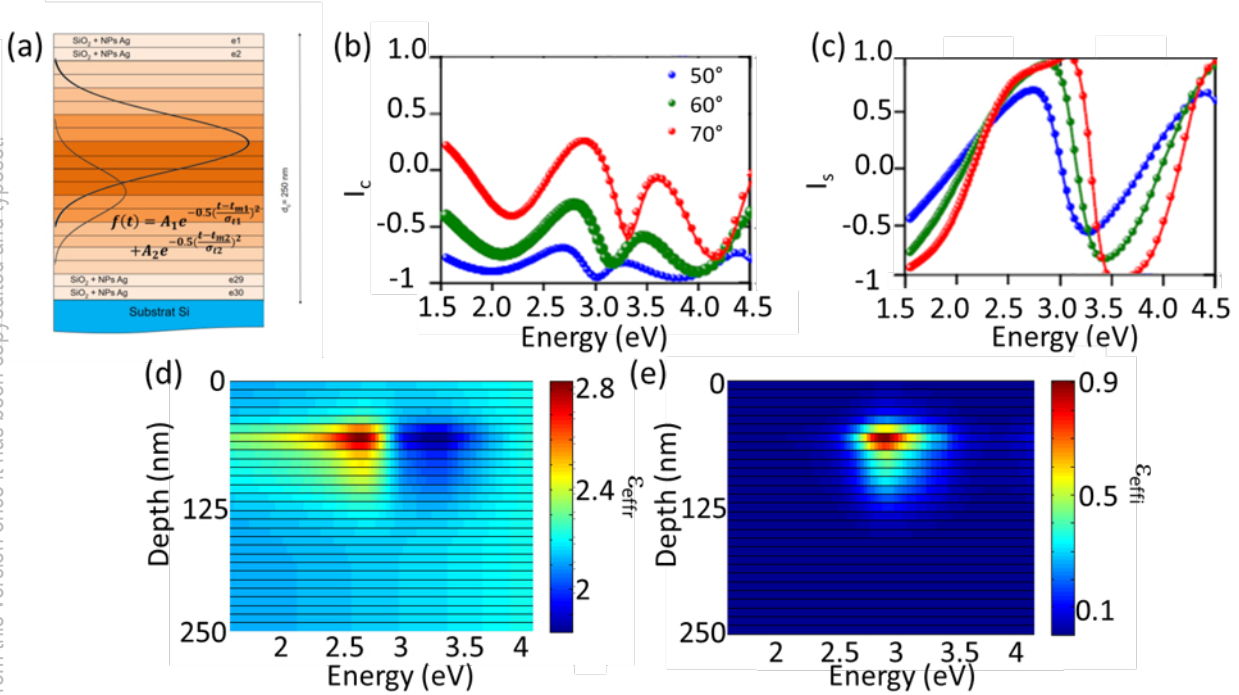

Journal of Vacuum Science Technology B

ACCEPTED MANUSCRIPT

This is the author's peer reviewed, accepted manuscript. However, the online version of record will be different from this version once it has been copyedited and typeset.

PLEASE CITE THIS ARTICLE AS DOI: 10.1116/1.5121343

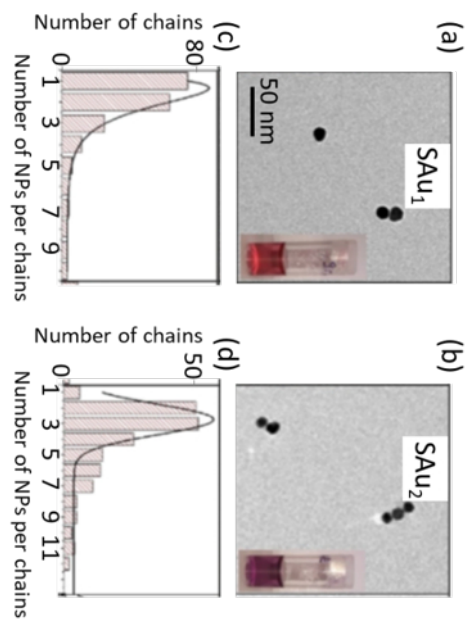

ACCEPTED MANUSCRIPT

Journal of Vacuum Science Technology B

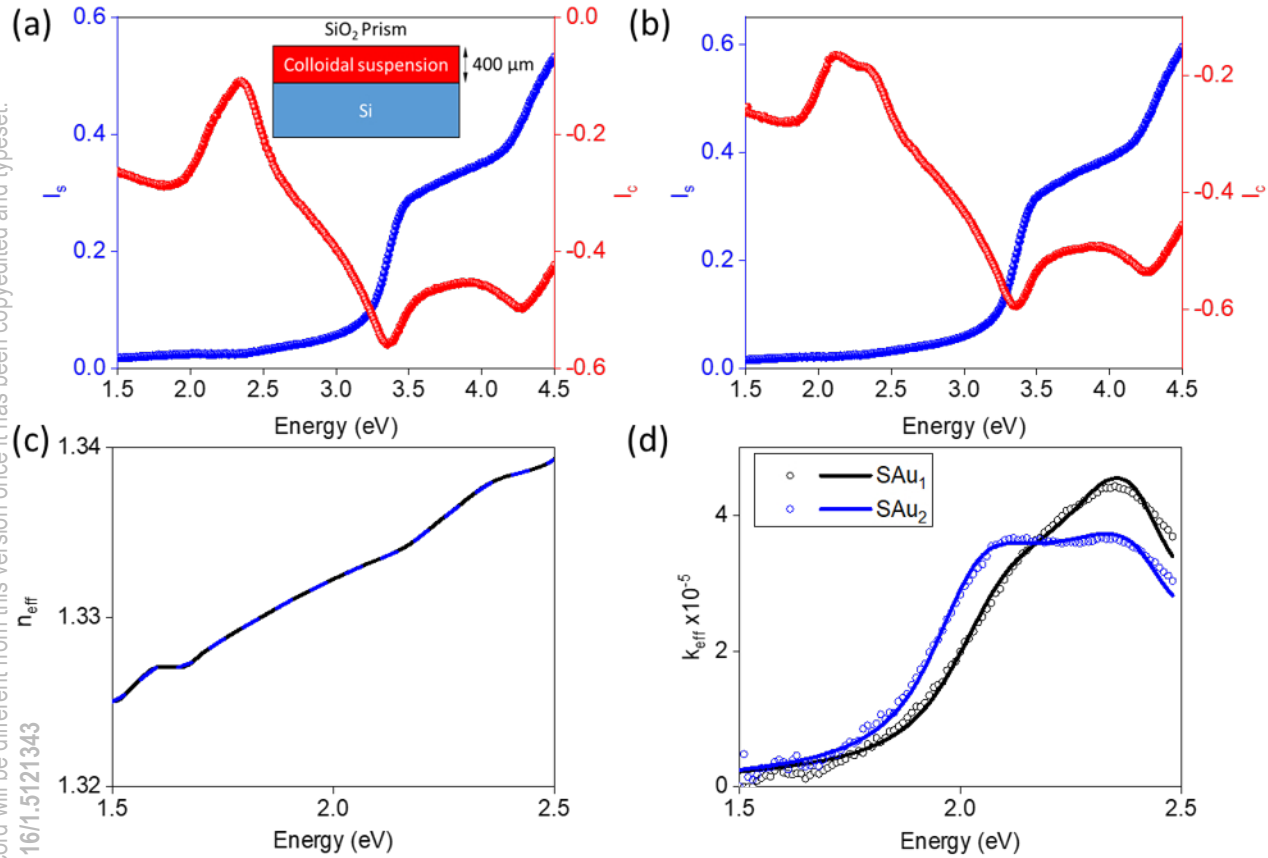

This is the author's peer reviewed, accepted manuscript. However, the online version of record will be different from this version once it has been copyedited and typeset.
PLEASE CITE THIS ARTICLE AS DOI: 10.1116/1.5121343

ACCEPTED MANUSCRIPT

Journal of Vacuum Science Technology B

This is the author's peer reviewed, accepted manuscript. However, the online version of record will be different from this version once it has been copyedited and typeset.
PLEASE CITE THIS ARTICLE AS DOI: 10.1116/1.5121343